Accepted Manuscript

Significance of grain refinement on microstructure and mechanical properties of an Al-3% Mg alloy processed by high-pressure torsion

Han-Joo Lee, Jae-Kyung Han, Shravan Janakiraman, Byungmin Ahn, Megumi Kawasaki, Terence G. Langdon

PII: S0925-8388(16)31917-X

DOI: 10.1016/j.jallcom.2016.06.194

Reference: JALCOM 38063

To appear in: *Journal of Alloys and Compounds*

Received Date: 7 April 2016

Revised Date: 10 June 2016

Accepted Date: 20 June 2016

Please cite this article as: H.-J. Lee, J.-K. Han, S. Janakiraman, B. Ahn, M. Kawasaki, T.G. Langdon, Significance of grain refinement on microstructure and mechanical properties of an Al-3% Mg alloy processed by high-pressure torsion, *Journal of Alloys and Compounds* (2016), doi: 10.1016/j.jallcom.2016.06.194.

Submitted to Journal of Alloys and Compounds (April 2016): Revised: June 2016

Significance of grain refinement on microstructure and mechanical properties of an Al-3% Mg alloy processed by high-pressure torsion

Han-Joo Lee[1], Jae-Kyung Han[1], Shravan Janakiraman[2], Byungmin Ahn[3*], Megumi Kawasaki[1,4*], Terence G. Langdon[4,5]

[1] Division of Materials Science and Engineering, Hanyang University, Seoul 133-791, Korea
[2] Siemens Wind Power A/S, Borupvej 16, 7330 Brande, Denmark
[3] Department of Energy Systems Research, Ajou University, Suwon 443-749, Korea
[4] Departments of Aerospace & Mechanical Engineering and Materials Science University of Southern California, Los Angeles, CA 90089-1453, U.S.A.
[5] Materials Research Group, Faculty of Engineering and the Environment University of Southampton, Southampton SO17 1BJ, U.K.

Abstract

Significant grain refinement is attractive for improving mechanical properties at both ambient and elevated temperatures and improvements in the properties of light-weight metals has become indispensable for the practical and societal needs of materials selection. Experiments were conducted to examine the influence of grain refinement on the mechanical properties of an Al-3% Mg alloy processed though high-pressure torsion (HPT) at room temperature under a compressive pressure of 6.0 GPa for up to 10 turns. The hardness values from Vickers microhardness measurements demonstrated a strain hardening behavior with increasing torsional straining and a high level of homogeneous microstructure was achieved along the disk diameter after HPT for 10 turns. An X-ray diffraction analysis at the peripheral regions of the disks outside of the central areas showed an evolution towards a reasonably random texture together with increases in the dislocation density and lattice parameter of Al with increasing numbers of HPT revolutions. A maximum elongation of ~430% was recorded in the alloy after HPT for 5 turns when testing at 673 K at 1.0×10^{-4} s^{-1} but there was evidence for grain growth during testing and the flow behavior was controlled by viscous glide. Analysis shows that the improved hardness through HPT is well expressed by the Hall-Petch relationship with only limited contributions from solid solution strengthening and precipitation hardening.

Keywords: aluminum alloy; deformation mechanisms; hardness; high-pressure torsion; strengthening mechanisms

*Corresponding authors: Megumi Kawasaki; megumi@hanyang.ac.kr; Tel: +82-2-2220-0404; Fax: +82-2-2298-4101, Byungmin Ahn; byungmin@ajou.ac.kr; Tel: +82-31-219-3531; Fax: +82-31-219-1613

1. Introduction

Ultrafine-grained (UFG) materials and bulk nanostructured materials (BNM) having ultrafine to true nanometer grains can be fabricated by severe plastic deformation (SPD) which is a promising technique for achieving grain refinement in bulk metals and alloys [1]. Among the various available SPD techniques, high-pressure torsion (HPT) provides the potential for achieving true nanostructures [2]. In this procedure, a disk is strained under a high compressive pressure with concurrent torsional straining and the processing is usually conducted at room temperature (RT) [3]. The processed metals generally demonstrate an enhancement of the physical and mechanical characteristics through significant grain refinement and the intensive introduction of point and line defects. Recent reviews described the importance of the different types of defects produced though SPD processing and the superior properties that may be achieved in UFG materials [4,5].

It is well established that the grain size is an exceptionally important structural parameter in polycrystalline metals. In practice, at low or ambient temperatures, typically at temperatures of $<0.5T_m$ where T_m is the absolute melting temperature, the measured yield stress, σ_y, varies with the grain size, d, through the Hall-Petch relationship which is given by [6,7]

$$\sigma_y = \sigma_o + k_y d^{-1/2} \qquad (1)$$

where σ_o and k_y are the friction stress and a yielding constant, respectively. It follows from eq (1) that a reduction in grain size leads to a major increase in the overall strength of the material and thus SPD processing is a promising technique especially for light-weight structural materials where a specific strength is indispensable [8]. The situation at elevated temperatures is different because, if the very small grain sizes introduced by SPD processing are reasonably stable at high temperatures, there is a potential for achieving significant grain boundary sliding and high superplastic ductilities [9].

The present study was initiated to examine the evolution in microstructure and mechanical properties, especially in hardness and the high temperature tensile properties, in an Al-3% Mg alloy processed by HPT at RT. Special emphasis was placed on evaluating the importance of strengthening through grain refinement by considering the contributions from other possible mechanisms for simple solid solution alloys such as solution strengthening and precipitation hardening. In addition, the tensile testing results were analyzed to evaluate the dominant deformation mechanism for the Al-Mg alloy after HPT when testing at a high temperature.

2. Experimental material and procedures

The experiments were conducted using an Al-3% Mg alloy containing small amounts (<0.003%) of Si and Fe impurities. The alloy was supplied as billets with diameters of 10 mm and lengths of ~65 mm and these billets were annealed at 773 K for 1 hour to give an average grain size of ~830 μm. A billet was cut into disks with ~1 mm thicknesses and each disk was carefully ground to have a final thickness of ~0.83 mm. The disks were then processed by HPT at RT under quasi-constrained conditions [10] using a compressive pressure of 6.0 GPa and a rotation speed of 1 rpm following the conventional procedure described elsewhere [11]. Thus, a set of disks was processed by only compression and also with compression and concurrent torsion to have total rotations, *N*, of 1/4, 1/2, 1, 5 and 10 turns.

The surfaces of the processed disks were polished with abrasive papers and then further polished with diamond paste on cloths to achieve mirror-like appearances. The Vickers microhardness value, Hv, was measured along the diameters on the polished disk surfaces after HPT using a Shimadzu HMV-2E microhardness tester with a load of 100 gf and a dwelling time of 10 s. In practice, following the procedure described earlier [11], the

hardness variation was examined along the disk diameter with a constant separation of 0.3 mm on each processed disk.

The crystallographic evolution was examined by X-ray diffraction (XRD) analysis using a Rigaku UltimaIV XRD with a radiation of Cu Kα at a scanning speed of 2° per min and 0.01° intervals. As demonstrated earlier, it is common to have large microstructural and texture differences between the center and edge regions of the disks after HPT [12] and therefore a small hole with a diameter of 3 mm was punched in the center of each repolished disk after hardness testing in order to evaluate the crystallographic characteristics only from the region that was well-deformed by torsional straining in each processed disk. The values of the lattice parameter, a, dislocation density, ρ, and mean crystallite size, $\langle x \rangle_{area}$, were determined from the XRD patterns for the as-annealed alloy prior to HPT and at the edge regions of the disks processed by HPT. These calculations used an XRD data analysis software, Materials Analysis Using Diffraction (MAUD) [13], which is based on a full pattern fitting procedure (Rietveld method) with an accuracy of a few percent.

The deformation behavior of the Al-3% Mg alloy was examined at a high temperature by tensile testing after HPT processing through 5 and 10 turns. A set of miniature tensile specimens was cut from the disks with gauge lengths and widths of 1 mm using electro-discharge machining (EDM). In practice, two separate tensile specimens were machined from off-center positions in each disk as demonstrated in an earlier report [14], thereby minimizing any effects that may be introduced by the occurrence of microstructural inhomogeneities near the center of each disk. For comparison purposes, a set of similar miniature specimens was also prepared from the as-annealed alloy prior to HPT processing.

All miniature specimens were pulled to failure in tension at a temperature of 673 K using an Instron testing machine equipped with specially designed specimen holders operating at a constant rate of crosshead displacement and with initial stain rates in the range

from 1.0×10^{-4} to 1.0×10^{-2} s^{-1}. Although there were minor differences in the specimen thicknesses after HPT, measurements of the cross-sectional areas of the gauge lengths were recorded prior to mechanical testing to provide accurate values for the flow stresses.

3. Experimental results

3.1 Vickers microhardness variations

The disks of the Al-3% Mg alloy were examined after HPT under 6.0 GPa for up to 10 turns and the Vickers microhardness variations along the disk diameters are shown in Fig. 1 where the lower dashed line denotes the hardness value of Hv ≈ 50 for the as-annealed sample prior to HPT. It should be noted that pure Al and Al alloys are typical materials showing reasonable hardness homogeneity through the height directions of the disks after HPT processing [15-17] and thus there is no influence of the measurement sections within the disk height on the hardness variations along the disk diameters.

It is apparent that, by comparison with the as-annealed condition, there are high hardness values throughout the disk diameter in the early stage of HPT though 1/4 turn. Except after 10 turns, most disks showed typical hardness gradations due to strain hardening behavior [18] where the lower hardness at the disk center increases towards the disk edge with increasing equivalent strain in HPT where the strain is given by $2\pi Nr/h\sqrt{3}$ [3] where N is the number of HPT revolutions and r and h are the radius and thickness of the disk, respectively. Specifically, there is a large difference in hardness between the disk center having Hv ≈ 75 and the disk edge having Hv ≈ 120 after 1/4 turn. With increasing numbers of turns, the hardness values both at the disk centers and edges increase gradually and reach ~100 and ~180 at the center and edge, respectively, after 5 turns. Thereafter, the hardness attained a consistent value of Hv ≈ 180 throughout the disk diameter after 10 turns, thereby demonstrating hardness evolution towards homogeneity over the Al-Mg disk surface after HPT though 10 turns.

The saturated value of hardness in the present Al-3% Mg alloy is consistent with the alloy in the same composition after HPT under 5 GPa [19] but the result is higher than the hardness value of ~130 after ECAP at RT [19,20]. Recent reports recorded that an Al-1% Mg alloy processed through HPT under 6.0 GPa after >3 turns demonstrated a hardness homogeneity with Hv ≈ 110 [21] and an Al-5% Mg alloy showed a homogeneous distribution of hardness with Hv ≈ 240 after HPT at 6.0 GPa for 10 turns [22]. These results, when considered together with the present hardness experiments, demonstrate that higher Mg contents lead to higher hardness values in homogeneity through HPT and this trend continues up to at least 10% of Mg in the Al matrix after 10 HPT turns [23].

3.2 Microstructural evolution

The microstructural evolution was observed by TEM and representative microstructures are displayed in Fig. 2 for the Al-3% Mg alloy after HPT for, from the left, 1/4, 1, 5 and 10 turns. In each disk, the microstructures were taken at the plane parallel to the disk surface near the center at $r \approx 0$ mm shown in Fig. 2 in the upper row and close to the edge at $r \approx 3.5$ mm shown in the lower row. All of the micrographs displayed in Fig. 2 were taken using a consistent magnification to provide a direct comparison of the evolution of the local microstructures after HPT processing through increasing HPT revolutions.

After HPT for 1/4 turn, there is a random non-cellular microstructure with many dislocations within coarse grains at the disk center whereas there are defined boundaries forming insufficiently equiaxed grains at the disk edge. Through one HPT turn, the central region appears to have a cellular structure whereas the boundaries are obscure and this contrasts with the ultrafine microstructure with well-defined grain boundaries at the disk edge. The occurrence of diffuse grain boundaries is well established in SPD processing and it is due to the introduction of non-equilibrium grain boundaries having an excess of extrinsic dislocations [24]. After additional revolutions to five turns, there remains many dislocations

forming thick boundary widths of grain boundaries for equiaxed small grains at $r \approx 0$ mm whereas the microstructure at the edge region is very similar to the microstructure after one turn. By contrast, the grain boundaries are well-defined and reasonably equiaxed ultrafine grains were observed at the central region after 10 turns and the ultrafine microstructure at the edge remained essentially the same as the microstructure after 5 turns. The microstructure at the center after 10 turns was now similar to the microstructure at the edge of the disk.

The detailed mean spatial grain sizes determined directly from the TEM micrographs are shown in Table 1 for the centers and edges of the disks after HPT for 1/4, 1, 5 and 10 turns. In addition, the grain size distributions at the disk edges were evaluated with increasing equivalent strain and the result is shown in Fig. 3. It is apparent in Table 1 that the microstructure at the edge region is finer than the central region in each processing revolution due to the higher torsional straining during HPT. Nevertheless, in both regions significant changes in grain size occur in the early stage of HPT up to 1 turn and there are further gradual changes in the central regions to reach a grain size of ~190 nm through 10 turns whereas there are only minor changes in the edge regions through 1 to 10 turns leading to a final grain size of ~180 nm.

The trend of saturation in grain size at the edge after 1 turn through HPT is also visible in Fig. 3 where the edge region at $r \approx 3.5$-4.0 mm receives an equivalent strain of ~17 after 1 turn. Ultimately, as shown in Fig. 2, there are very similar microstructures both at the center and the edge of the disk after 10 turns and thus these observations confirm that there is a significant level of microstructural evolution towards homogeneity with increasing numbers of turns up to 10. The microstructural homogeneity after 10 turns is in direct correlation with the hardness homogeneity in the same alloy after HPT as shown in Fig. 1. From an initial grain size of ~830 μm, processing through HPT produced significant grain refinement to

minimum grain sizes of ~180-190 nm in the Al-3% Mg alloy. This refinement in grain size is consistent with numerous other reports of the grains sizes produced in various Al-Mg alloys after processing by HPT at RT [19,21-23,25-31] as documented in Table 2.

3.3 Texture and crystallographic variations

Figure 4 shows the variations of the XRD profiles within a limited angular range, 2 theta, of 31°-50° measured for the Al-3% Mg alloy where the samples are, from the top, after compression under 6.0 GPa for 1 min without torsional straining and then after HPT for 1/4, 1/2, 1, 5 and 10 turns. The arrangement of atoms within the unit cell is associated with the relative intensities of the XRD peaks and thus it is anticipated that the two strongest intensities on the (111) and (200) planes will appear within the examined angular range in the XRD profiles for Al alloys including the present Al-3% Mg alloy. For a direct comparison, the relative peak intensities of the peaks at the (200) plane are fixed constant for all sample conditions. An examination of the XRD profiles in Fig. 4 shows there are peaks only for pure Al without any Al-Mg compounds and there is no significant change with increasing numbers of HPT revolutions except that the sample subjected only to compression exhibits a lower relative intensity at the (111) lattice plane.

In order to quantitatively evaluate the texture change in the Al-3% Mg alloy with increasing numbers of HPT turns, the XRD profiles in Fig. 4 were further analyzed in terms of the normalized peak intensity, K_i, where i denotes an arbitrarily selected crystal plane for the diffraction maxima. First, the relative peak intensity, J_i, for the (111) plane was calculated by comparison with the (200) plane using the following definition:

$$J_{111} = \frac{I_{111}}{I_{111} + I_{200}} \qquad (2)$$

where I_{hkl} is the X-ray peak intensity of the (hkl) plane shown in Fig. 4. The experimentally calculated value through the XRD analysis provides $J_{111,exp}$ and this is then compared with $J_{111,random}$ for the relative intensity in the theoretical random lattice orientation of Al where

$J_{111,random}$ = 0.68 obtained from the diffraction database installed in the XRD facility. Accordingly, the normalized peak intensity for the (111) plane, K_{111}, is defined in the following form:

$$K_{111} = \frac{J_{111,exp}}{J_{111,\,random}} \tag{3}$$

Thus, a K value of 1.0 implies a consistency in the X-ray intensities observed between the experiments and a random orientation of an f.c.c. crystal lattice in terms of the selected slip plane.

Although these calculations involve only the two major orientations for Al of an f.c.c. crystal, the analysis specifically emphasizes the relative texture change at the peripheral regions of the disks with increasing HPT turns. Thus, the K_i values were estimated for the two major planes of (111) and (200) and the results are summarized in Fig. 5 for the samples examined through XRD as documented in Fig. 4 where the sample subjected only to compression is designated by N = 0. This approach was demonstrated in an earlier report considering texture evolution in an AZ31 magnesium alloy under different testing histories [32] and recently it was applied to a ZK60 magnesium alloy processed through HPT [12].

For the compression stage, it is apparent from Fig. 5 that the (200) plane lies parallel to the limited outward flow of material which occurs in a radial direction due to the quasi-constrained HPT processing whereas there are fewer (111) planes lying parallel to the disk surface which explains the lower (111) peak intensity after compression. With increasing numbers of turns to 1, the strong texture observed in the compression stage is reduced and it becomes very close to the theoretically random texture which was achieved after 5 turns by HPT. Thereafter, the ideal random texture in the Al-Mg alloy tends to have a preferred texture with more (200) planes lying parallel to the disk surface after HPT through 10 turns.

A similar texture change was demonstrated earlier with pole figures at the (111) and (200) planes for an Al-5.9% Mg- 0.3% Sc alloy after HPT for 1, 5 and 10 turns [31].

The XRD patterns taken at the peripheral regions of the disks were examined using the MAUD software. The results are shown in Fig. 6 for the measured change in the lattice parameter of Al with the numbers of turns and in Fig. 7 for the evolution of the dislocation density and the area-weighted mean crystallite size, $\langle x \rangle_{area}$, at the peripheral regions of the disks with increasing numbers of HPT revolutions and therefore with equivalent strain. It should be noted that this approach is especially useful for describing the indistinguishable microstructural evolution shown in the XRD profiles.

The variation in the lattice parameter with increasing HPT turns is shown in Fig. 6 where $N = 0$ corresponds to the sample under compression without torsion straining and the lattice parameter of 4.06827 Å denoted by a broken line is for the Al-3% Mg alloy after annealing but prior to compression and HPT processing. It is apparent that all lattice parameters measured for the processed samples shows are lower than for the as-annealed sample. Nevertheless, compression without torsion produces the smallest lattice parameter in the alloy and thereafter the parameter increases significantly through 1 turn, reaches a maximum after 5 turns and then remains constant up to 10 turns. The saturation in the lattice parameter of the Al-3% Mg alloy after 5 turns is in reasonable agreement with estimated values from pure Al and Al-5% Mg and Al-10% Mg alloys after HPT for an equivalent strain of 300 where it was shown that the saturation lattice parameter became wider with increasing Mg content in the aluminum matrix [33].

The dislocation density, ρ, was determined using the following relationship developed originally for powder materials using the dislocation densities calculated from the particle size, ρ_p, and from strain broadening, ρ_s [34]:

$$\rho = \left(\rho_p \rho_s\right)^{1/2} = \left[\left(\frac{3n}{D_m{}^2}\right) \cdot \left(\frac{k\xi^2}{F\mathbf{b}^2}\right)\right]^{1/2} \quad (4)$$

where D_m is the dimension of a refined block separated by dislocations lying on the boundaries within a well-worked metal, n is the number of dislocations per block face and takes 1 for very severely deformed metals including randomly distributed dislocations, k is a constant which takes a value of ~24 [34], F is an interaction factor taken as ~1 by assuming one dislocation coincides with the edge of each block, ξ is the microstrain obtained through MAUD, and **b** is the Burgers vector where **b** = 2.86×10^{-10} m for pure Al [35].

The evolution of the dislocation density and the mean crystallite size is shown in Fig. 7 where the compression sample is designated by N = 0 and the sample in the as-annealed condition prior to HPT processing gave $\rho \approx 1.13 \times 10^{13}$ m^{-2} and $\langle x \rangle_{area} \approx 355$ nm. It is readily apparent from Fig. 7 that the dislocation density increased by about one order of magnitude after compression without torsion by comparison with the as-annealed condition, it then increased continuously towards $>3.7 \times 10^{14}$ m^{-2} up to HPT for 1 turn and thereafter remained reasonably constant up to 10 HPT turns. The measured saturation dislocation density after 1 turn is in good agreement with a recent report for an Al-1% Mg alloy after HPT through 10 turns [21]. As described in an earlier report [36], the mean crystallite size determined by XRD analysis is generally smaller than the grain sizes measured using TEM micrographs as shown in Fig. 2. In practice, the measured crystallite size was reduced from ~355 nm in the as-annealed condition to ~110 nm by compression prior to torsion and this value remained reasonably constant though HPT up to 10 turns. This trend is also consistent with earlier reports for an Al-1% Mg alloy after HPT through 1 to 10 turns [21] and an Al-3% Mg alloy after ECAP for a true strain of >1 [36].

3.4 High temperature tensile properties

Tensile testing was conducted at 673 K at initial strain rates of $1.0 \times 10^{-4} – 1.0 \times 10^{-2}$ s^{-1} after HPT processing through 5 and 10 turns which produces reasonably homogeneous hardness distributions and microstructures at the off-center positions as documented in Figs 1-3 and Table 1. For comparison purposes, the miniature tensile specimens of the as-annealed alloy prior to compression and HPT were tested under the same conditions.

A series of tests was conducted and a representative example of engineering stress-strain curves is shown in Fig. 8 for an initial strain rate of 1.0×10^{-3} s^{-1} and at a temperature of 673 K. For direct comparison, the as-annealed Al-Mg alloy without HPT was machined into the same miniature specimens and tested under the same conditions. It is apparent that the samples after HPT for 5 and 10 turns showed very similar creep flow with uniform deformation leading to higher ductility in contrast to the as-annealed sample showing higher engineering stress and lower ductility under the high temperature of testing.

Fig. 9 shows plots of the measured elongations to failure (upper) and measured flow stresses (lower) versus strain rate for the alloy in the annealed condition and after HPT for 5 and 10 turns; for the lower plot, the 0.2% offset yield stress was taken as the flow stress for each sample. It is apparent from Fig. 9 that the elongations increase with decreasing strain rate for all samples but the alloy consistently exhibits the highest elongations at all strain rates after 5 turns whereas the lowest elongations are recorded in the as-annealed condition. A highest elongation of ~430% was recorded in the alloy at the lowest strain rate after 5 turns whereas the elongations were close to ~400% and ~320% after 10 turns and in the as-annealed condition, respectively. The lower elongations in the disk for the 10 HPT turns are due to the occurrence of faster grain growth at the high testing temperature where the faster grain growth is attributed to the presence of higher fractions of high-angle grain boundaries with increasing numbers of HPT turns [37-39] whereas no significant change in grain size was observed in the Al-Mg alloys after 5 turns as shown in Figs 2 and 3 and Table 1.

The lower plot in Fig. 9 shows there is no significant difference in the values of stress for the alloy before and after HPT for 5 and 10 turns and the measured strain rate sensitivity, *m*, is ~0.35 over the present range of strain rate. Since conventional superplasticity requires elongations of at least 400% [40], it appears that the Al-3% Mg alloy processed by HPT for 5 turns is essentially at the limiting condition for superplastic flow at the slowest strain rate of 1.0×10^{-4} s^{-1}. Furthermore, inspection showed there was reasonably uniform deformation within the gauge length under these testing conditions and this is consistent with superplastic flow which requires neck-free deformation within the gauge length [41].

Nevertheless, the alloy failed to achieve good superplastic properties in these tests and microstructural inspection showed this was due to the occurrence of dynamic grain growth at the testing temperature of 673 K. Thus, annealing samples for 1 hour at 673 K led to spatial grain sizes of ~50 and ~55 μm after HPT processing through 5 and 10 turns, respectively, where the larger grain growth after 10 turns accounts for the lower elongations recorded in these samples in Fig. 9. Furthermore, annealing for 1 hour at 673 K gave a Vickers microhardness of Hv ≈ 50 after 10 turns of HPT processing where this hardness is similar to the initial hardness prior to HPT. These grain sizes and hardness values are consistent with earlier reports for an Al-3% Mg alloy processed either by ECAP to a strain of ~4 [19,20] or by HPT to a logarithmic strain of ~7 [19] and with subsequent static annealing at 673 K for 1 hour.

4. Discussion

4.1 High temperature mechanical properties

In the tensile testing conducted in this investigation, the highest elongation of ~430% was obtained for the Al-3% Mg alloy after HPT for 5 turns and testing at 673 K at 1.0×10^{-4} s^{-1}. Nevertheless, the results do not show good superplastic flow because of the advent of significant grain growth in the tensile tests conducted at a temperature of 673 K. This result

is consistent with earlier studies of the microstructural stability of the Al-3% Mg alloy where it was shown that a temperature of ~500 K was the upper limiting temperature for testing this alloy in order to make use of the UFG microstructure [42]. Furthermore, the strain rate sensitivity of $m \approx 0.35$ in Fig. 9 is not consistent either with the occurrence of grain boundary sliding in superplasticity [43] or with the predictions for conventional superplastic flow where $m \approx 0.5$ [9,44].

In order to identify the appropriate deformation regime of the alloy under the tensile testing conditions which generally cover intermediate to high stress regimes in creep, a logarithmic plot of strain rate versus stress is generally constructed for measuring a stress exponent, *n*, where the plot is the reciprocal of the lower plot in Fig. 8. Thus, from the slope of the line exhibiting *m* in Fig. 9, a stress exponent of $n \approx 3.0$ is calculated for all datum points of the Al-Mg alloy after HPT. This value is in excellent agreement with numerous earlier reports for coarse-grained Al-Mg alloys deforming by viscous glide where the rate-controlling process is the dragging of solute atom atmosphere by the moving dislocations: for example, this behavior was reported for aluminum-based solid solution alloys tested at temperatures of 573-673 K under intermediate to high stress conditions of ~10 to $<10^2$ MPa [45-52].

It is important to note that the testing conditions used in this investigation are significantly lower than the normal power-law breakdown which occurs at high stresses at a normalized strain rate of $\dot{\varepsilon}/D \approx 10^{13}$ m^{-2} where *D* is the appropriate diffusion coefficient for pure metals and dilute solutions [53]. In practice, there are two diffusion coefficients available for the dilute Al-Mg alloy: $\tilde{D}$ for diffusivity of Mg atoms in the Al matrix given by 1.24×10^{-4} exp (-130.5/*RT*) m^2 s^{-1} [54] and D_l for lattice self-diffusion in pure Al given by 1.86×10^{-4} exp (-143.4/*RT*) [42] where *R* is the gas constant. At 673 K, these diffusion coefficients lead to $\dot{\varepsilon}/\tilde{D} \approx 1.1\times10^{12}$ m^{-2} and $\dot{\varepsilon}/D_l \approx 7.2\times10^{12}$ m^{-2} at the highest strain rate of

1.0×10^{-2} s^{-1} and these values show that the flow behavior of the alloy lies entirely within the viscous glide region for the present experimental conditions so that there is no power-law breakdown.

It is worth noting that, although the Al-3% Mg alloy in the present study failed to demonstrate true superplasticity at 673 K due to grain growth, Al-Mg alloys have a significant potential for achieving excellent superplastic ductilities especially when additions such as Sc and/or Zr are introduced to maintain an ultrafine-grained microstructure. For example, Al-3% Mg alloys with additions of Sc [55-65] and both Sc and Zr [64,66,67] demonstrated excellent superplastic elongations of up to >2000% at temperatures in the range of 573-723 K using strain rates of ~10^{-4} - 1.0 s^{-1} after processing though ECAP for 6-8 passes. Superplastic ductilities of up to ~1600% were also achieved in similar alloys with Sc additions after processing by HPT [27,68,69]. Comprehensive reviews have tabulated large numbers of results describing superplasticity in metals after SPD processing including various Al alloys processed by ECAP [70] and HPT [9] and a recent review provides additional experimental data and describes the importance of microstructural homogeneity in UFG metals for achieving superplastic properties [71].

4.2 An analysis of strengthening mechanisms

Processing though HPT demonstrates the advent of significant grain refinement from ~830 μm to ~180 nm in the Al-3% Mg alloy after HPT through 10 turns as shown in Fig. 2 and Table 1. The refined microstructure exhibits improved hardness tending towards homogeneity after 10 turns with a measured hardness across the disk of Hv ≈ 180 as shown in Fig. 1. This significant increase in hardness may be explained by Hall-Petch strengthening as given in eq (1) when the relationship is reformulated in terms of hardness in the form

$$H = H_0 + k_H d^{-1/2} \quad (5)$$

where H is the hardness and H_0 and K_H are the appropriate material constants associated with the hardness measurements. The validity of utilizing the Hall-Petch relationship in eqs (1) and (5) was demonstrated in an earlier report using Al-3% Mg and Al-5.5% Mg-2.2% Li-0.12% Zr alloys after processing by ECAP [20].

Applying the relationship in eq (5), the Vickers microhardness values in Fig. 1 were re-plotted as a function of $d^{-1/2}$ for the Al-3% Mg alloy in an as-annealed condition without HPT, after HPT for 1/4, 1, 5 and 10 turns at the edge and center positions and after HPT followed by static annealing at 673 K for 1 h. The plot is shown in Fig. 10 where additional datum points are also included for a similar Al-3% Mg alloy processed either by ECAP [20] or HPT [19].

This analysis confirms that there is a conventional linear relationship between hardness and $d^{-1/2}$ for all sample conditions in the present Al-3% Mg alloy from coarse grain sizes in the initial condition and after annealing to ultrafine grain sizes after HPT. In practice, all of the experimental points lie close to a single line given by eq (5) with H_0 = 59.7 Hv and $K_H \approx 43.3$ Hv $\mu m^{-1/2}$. This relationship with grain sizes ranging down to ~180 nm is in good agreement with earlier results on a similar alloy after ECAP and HPT where it was reported that $H_0 \approx$ 46-47.5 Hv and $K_H \approx$ 35.0-41.0 Hv $\mu m^{-1/2}$ [19,20]. However, the earlier results demonstrated a possible decrease in slope at grain sizes in the range of ~0.09-0.15 µm after processing by HPT where there was a decrease to $K_H \approx 10.0$ Hv $\mu m^{-1/2}$ [19]. As shown in recent investigations of dilute Al-Mg alloys processed by HPT [22,25], the present Al-Mg alloy exhibits excellent Hall-Petch strengthening through grain reduction.

Considering the essential characteristics of dilute Al-Mg alloys, there is a limited solubility of Mg in the Al matrix and the non-dissolved Mg exists in the form of Mg-rich clusters in a phase of an Al_3Mg_2 intermetallic. However, the XRD analysis failed to detect this phase which implies that the quantity of the phase is very small and <5 vol.%. The

finding of an intermetallic phase was reported after HPT using high-resolution TEM on Al-5% Mg and Al-10% Mg alloys but these studies also failed to detect the existence of the intermetallic phase using XRD analysis [23,33].

The change in the lattice parameter of Al as shown in Fig. 6 at the peripheral regions of the disks provides an indirect estimate of the Mg solubility in the Al solid solution [72]. The results are summarized in the upper row of Table 3 where the initial as-annealed condition prior to HPT showed an Mg concentration of ~4.3 ± 0.3 at.% in the Al solid solution. It should be noted that the actual Mg concentration in the Al solid solution tends to be higher than the nominal composition of Al-Mg alloy [29]. Thus, the reduction of the Mg concentration by compression and in the very early stages of HPT leads to a deformation-induced segregation or precipitation of an Mg-rich phase at the grain boundaries which is reasonably consistent with results from an Al-Mg alloy containing a high Mg content of >5.5 at.% after HPT [4,29]. The Mg decomposition from the solid solution causes softening of the Al-Mg alloy after HPT by comparison with the coarse-grained alloy [23]. However, the Mg content increases with increasing numbers of turns in the dilute Al-Mg alloy used in these experiments so that there is dissolution of Mg atoms in the solid solution which gives a solution strengthening in addition to the Hall-Petch strengthening.

As demonstrated earlier in a diffusion-bonded Al-Mg system processed by HPT using separate Al and Mg disks [73], the observed high hardness in the Al-3% Mg alloy is a consequence of strengthening by grain refinement together with solid solution strengthening and precipitation hardening [74]. The value of the hardness increase by solid solution hardening may be expressed in the form

$$\Delta Hv = 1/3 \times [H_{os} \times (\text{wt.\% Mg})] \quad (6)$$

where H_{os} is a constant taking values in the range of ~13.8-15.5 for Al-Mg alloys [75,76] by applying the general relationship between hardness and yield strength in MPa so that Hv =

$\sigma_y/3$ [77]. By applying the estimated Mg concentrations listed in the upper row of Table 3, the calculated results are shown in the two lower rows where the second row gives the hardness change by solid solution strengthening and the third row gives the contribution of solid solution strengthening to the total hardness at the edge regions as shown in Fig. 1 for samples after compression and after HPT through 1/4-10 turns. These calculations demonstrate that the improved hardness by solid solution strengthening is higher with increasing numbers of HPT revolutions. Nevertheless, the contribution of solid solution strengthening to the total hardness remains reasonably consistent at ~7-8% for all samples processed by HPT.

For precipitation hardening, it is difficult to estimate the significance from the present experimental results since, by assuming a homogeneous distribution of precipitates, any calculation requires information on the volume and size of the precipitates in the matrix [78]. However, an Mg-rich phase was not observed in these samples in any condition using either TEM or XRD thereby inferring there is an insignificant contribution from precipitation hardening in the Al-3% Mg alloy after HPT. Thus, the combination of solid solution strengthening and precipitation hardening is expected to account for <10% of the total hardness of the Al-3% Mg alloy and accordingly it is concluded that the Hall-Petch relationship provides a good and accurate description of the hardening of the Al-3% Mg alloy at very fine grain sizes. Thus, the Hall-Petch plot shown in Fig. 10 provides an excellent description of the increase in hardness by grain refinement in dilute Al-Mg alloys.

5. Summary and conclusions

1. An Al-3% Mg alloy was processed though HPT at room temperature under a pressure of 6.0 GPa and with torsional straining from 1/4 to 10 turns. The refinement of microstructure was confirmed after processing by microhardness measurements and microstructural analysis from the centers to the edges of the disks and by XRD analysis at

the peripheral regions of the disks. The high temperature tensile properties were also examined at 673 K.

2. There was a significant grain refinement from 830 μm prior to HPT to ~180-190 nm at both the center and edge of the disk processed thorough 10 turns. This extensive microstructural change increased the dislocation density and the lattice parameter especially in the early stages of HPT up to 1 turn.
3. After HPT for 5 turns, the alloy demonstrated a high elongation of ~430% at 673 K but large superplastic ductilities were not achieved because of the occurrence of significant grain growth. The experimental data gave a stress exponent of $n \approx 3.0$ for both coarse and submicrometer grains thereby demonstrating that flow occurred by viscous glide.
4. In principle, the improved hardness through HPT may be a consequence of the grain refinement, solid solution strengthening and precipitation hardening. However, it is shown that the contributions from solid solution and precipitation strengthening are essentially insignificant and the hardening is due to grain refinement strengthening. Thus, the Hall-Petch relationship is an appropriate description for the improved hardness in the Al-3% Mg alloy.

Acknowledgements

This research was supported in part by the NRF Korea funded by MoE under Grant No. NRF-2014R1A1A2057697 and 2016R1A6A1A03013422 (MK), in part by the NRF Korea funded by MSIP under Grant No. NRF-2015R1A2A2A01002387 (BA) and in part by the European Research Council under ERC Grant Agreement No. 267464-SPDMETALS (TGL).

References

[1] R.Z. Valiev, R.K. Islamgaliev, I.V. Alexandrov, Bulk nanostructured materials from severe plastic deformation, Prog. Mater. Sci. 45 (2000) 103-189.

[2] T.G. Langdon, Twenty-five years of ultrafine-grained materials: Achieving exceptional properties through grain refinement, Acta Mater. 61 (2013) 7035-7059.

[3] A.P. Zhilyaev, T.G. Langdon, Using high-pressure torsion for metal processing: Fundamentals and applications, Prog. Mater. Sci. 53 (2008) 893-979.

[4] X. Sauvage, G. Wilde, S.V. Divinski, Z. Horita, R.Z. Valiev, Grain boundaries in ultrafine grained materials processed by severe plastic deformation and related phenomena, Mater. Sci. Eng. A 540 (2012) 1-12.

[5] R.Z. Valiev, Y. Estrin, Z. Horita, T.G. Langdon, M.J. Zehetbauer, Y.T. Zhu, Fundamentals of superior properties in bulk NanoSPD materials, Mater. Res. Lett. 4 (2016) 1-21.

[6] E.O. Hall, The deformation and ageing of mild steel: III Discussion of results, Proc. Phys. Soc. B 64 (1951) 747-753.

[7] N.J. Petch, The cleavage strength of polycrystals, J. Iron Steel Inst. 174 (1953) 25-28.

[8] K. Lu, The future of metals, Science 328 (2010) 319-320.

[9] M. Kawasaki, T.G. Langdon, Review: achieving superplasticity in metals processed by high-pressure torsion, J. Mater. Sci. 49 (2014) 6487-6496.

[10] R.B. Figueiredo, P.R. Cetlin, T.G. Langdon, Using finite element modeling to examine the flow processes in quasi-constrained high-pressure torsion, Mater. Sci. Eng. A 528 (2011) 8198-8204.

[11] M. Kawasaki, T.G. Langdon, The significance of strain reversals during processing by high-pressure torsion, Mater. Sci. Eng. A 498 (2008) 341-348.

[12] H.-J. Lee, S.K. Lee, K.H. Jung, G.A. Lee, B. Ahn, M. Kawasaki, T.G. Langdon, Evolution in hardness and texture of a ZK60A magnesium alloy processed by high-pressure torsion, Mater. Sci. Eng. A 630 (2015) 90-98.

[13] L. Lutterotti, S. Matthies, H.-R. Wenk, MAUD: a friendly Java program for material analysis using diffraction, International Union of Crystallography: Newsletter of the Commission for Powder Diffraction 21 (1999) 14-15.

[14] A. Loucif, R.B. Figueiredo, M. Kawasaki, T. Baudin, F. Brisset, R. Chemam, T.G. Langdon, Effect of aging on microstructural development in an Al–Mg–Si alloy processed by high-pressure torsion, J. Mater. Sci. 47 (2012) 7815-7820.

[15] M. Kawasaki, R.B. Figueiredo, T.G. Langdon, An investigation of hardness homogeneity throughout disks processed by high-pressure torsion, Acta Mater. 59 (2011) 308-316.

[16] M. Kawasaki, R.B. Figueiredo, T.G. Langdon, Twenty-five years of severe plastic deformation: recent developments in evaluating the degree of homogeneity through the thickness of disks processed by high pressure torsion, J. Mater. Sci. 47 (2012) 7719-7725.

[17] M. Kawasaki, R.B. Figueiredo, Y. Huang, T.G. Langdon, Interpretation of hardness evolution in metals processed by high-pressure torsion, J. Mater. Sci. 49 (2014) 6586-6596.

[18] M. Kawasaki, Different models of hardness evolution in ultrafine-grained materials processed by high-pressure torsion, J. Mater. Sci. 49 (2014) 18-34.

[19] M. Furukawa, Z. Horita, M. Nemoto, R.Z. Valiev, T.G. Langdon, Microhardness measurements and the Hall-Petch relationship in an Al-Mg alloy with submicrometer grain size, Acta Mater. 44 (1996) 4619-4629.

[20] M. Furukawa, Z. Horita, M. Nemoto, R.Z. Valiev, T.G. Langdon, Factors influencing the flow and hardness of materials with ultrafine grain sizes, Philos. Mag. A 78 (1998) 203-216.

[21] O. Andreau, J. Gubicza, N.X. Zhang, Y. Huang, P. Jenei, T.G. Langdon, Effect of short-term annealing on the microstructures and flow properties of an Al-1% Mg alloy processed by high-pressure torsion, Mater. Sci. Eng. A 615 (2014) 231-239.

[22] P. Bazarnik, Y. Huang, M. Lewandowska, T.G. Langdon, Structural impact on the Hall-Petch relationship in an Al-5Mg alloy processed by high-pressure torsion, Mater. Sci. Eng. A 626 (2015) 9-15.

[23] A.A. Mazilkin, B.B. Straumal, E. Rabkin, B. Baretzky, S. Enders, S.G. Protasova, O.A. Kogtenkova, R.Z. Valiev, Softening of nanostructured Al-Zn and Al-Mg alloys after severe plastic deformation, Acta Mater. 54 (2006) 3933-3939.

[24] J. Wang, Z. Horita, M. Furukawa, M. Nemoto, N.K. Tsenev, R.Z. Valiev, Y. Ma, T.G. Langdon, An investigation of ductility and microstructural evolution in an Al-3% Mg alloy with sub micron grain size, J. Mater. Res. 8 (1993) 2810-2818.

[25] R.Z. Valiev, F. Chmelik, F. Bordeaux, G. Kapelski, B. Baudelet, The Hall-Petch relation in submicro-grained Al-1.5% Mg alloy, Scripta Metall. Mater. 27 (1992) 855-860.

[26] Y. Ma, Z. Horita, M. Furukawa, M. Nemoto, R.Z. Valiev, T.G. Langdon, Yield stress measurements on an Al-1.5% Mg alloy with submicron grain size using a miniature bending procedure, Mater. Lett. 23 (1995) 283-287.

[27] G. Sakai, Z. Horita, T.G. Langdon, Grain refinement and superplasticity in an aluminum alloy processed by high-pressure torsion, Mater. Sci. Eng. A 393 (2005) 344-351.

[28] Z. Horita, T.G. Langdon, Microstructures and microhardness of an aluminum alloy and pure copper after processing by high-pressure torsion, Mater. Sci. Eng. A 410-411 (2005) 422-425.

[29] X. Sauvage, N. Enikeev, R. Valiev, Y. Nasedkina, M. Murashkin, Atomic-scale analysis of the segregation and precipitation mechanisms in a severely deformed Al-Mg alloy, Acta Mater. 72 (2014) 125-136.

[30] R.Z. Valiev, N.A. Enikeev, M.Yu. Murashkin, V.U. Kazykhanov, X. Sauvage, On the origin of the extremely high strength of ultrafine-grained Al alloys produced by severe plastic deformation, Scripta Mater. 63 (2010) 949-952.

[31] S.V. Dobatkin, V.V. Zakharov, A.Yu. Vinogradov, K. Kitagawa, N.A. Krasil'nikov, T.D. Rostova, E.N. Bastarash, Nanocrystalline structure formation in Al-Mg-Sc alloys during severe plastic deformation, Russ. Metall. 2006 (2006) 533-540.

[32] H. Watanabe, M. Fukusumi, Mechanical properties and texture of a superplastically deformed AZ31 magnesium alloy, Mater. Sci. Eng. A 477 (2008) 153-161.

[33] B.B. Straumal, B. Baretzky, A.A. Mazilkin, F. Phillipp, O.A. Kogtenkova, M.N. Volkov, R.Z. Valiev, Formation of nanograined structure and decomposition of supersaturated solid solution during high pressure torsion of Al-Zn and Al-Mg alloys, Acta Mater. 52 (2004) 4469-4478.

[34] G.K. Williamson, R.E. Smallman, III. Dislocation densities in some annealed and cold-worked metals from measurements on the X-ray debye-scherrer spectrum, Phil. Mag. 1 (1956) 34-46.

[35] H.J. Frost, M.F. Ashby, Deformation-mechanism maps: The plasticity and creep of metals and ceramics, Pergamon Press, Oxford, UK, 1982.

[36] J. Gubicza, N.Q. Chinh, Z. Horita, T.G. Langdon, Effect of Mg addition on microstructure and mechanical properties of aluminum, Mater. Sci. Eng. A 387-389 (2004) 55-59.

[37] A. Loucif, R.B. Figueiredo, T. Baudin, F. Brisset, T.G. Langdon, Microstructural evolution in an Al-6061 alloy processed by high-pressure torsion, Mater. Sci. Eng. A 527 (2010) 4864.

[38] A. Loucif, R.B. Figueiredo, T. Baudin, F. Brisset, R. Chemam, T.G. Langdon, Ultrafine grains and the Hall–Petch relationship in an Al–Mg–Si alloy processed by high-pressure torsion, Mater. Sci. Eng. A 532 (2012) 139.

[39] A.Y. Khereddine, F.H. Larbi, H. Azzeddine, T. Baudin, F. Brisset, A.L. Helbert, M.H. Mathon, M. Kawasaki, D. Bradai, T.G. Langdon, Microstructures and textures of a Cu–Ni–Si alloy processed by high-pressure torsion, J. Alloys Compds 574 (2013) 361-367.

[40] T.G. Langdon, Seventy-five years of superplasticity: historic developments and new opportunities, J. Mater. Sci. 44 (2009) 5998-6010.

[41] T.G. Langdon, Fracture processes in superplastic flow, Metal Sci. 16 (1982) 175-183.

[42] J. Wang, Y. Iwahashi, Z. Horita, M. Furukawa, M. Nemoto, R.Z. Valiev, T.G. Langdon, An investigation of microstructural stability in an Al-Mg alloy with submicrometer grain size, Acta Mater. 44 (1996) 2973-2982.

[43] T.G. Langdon, An evaluation of the strain contributed by grain boundary sliding in superplasticity, Mater. Sci. Eng. A 174 (1994) 225-230.

[44] T.G. Langdon, A unified approach to grain boundary sliding in creep and superplasticity, Acta Metall. Mater. 42 (1994) 2437-2443.

[45] C.N. Ahlquist, W.D. Nix, The measurement of internal stresses during creep of Al and Al-Mg alloys, Acta Metall. 19 (1971) 373-385.

[46] K.L. Murty, F.A. Mohamed, J.E. Dorn, Viscous glide, dislocation climb and newtonian viscous deformation mechanisms of high temperature creep in Al-3Mg, Acta Metall. 20 (1972) 1009-1018.

[47] K.L. Murty, Transitional creep mechanisms in Al-5Mg at high stresses, Scripta Metall. 7 (1973) 899-903.

[48] K. Kuchařová, I. Saxl, J. Čadek, Effective stress in steady state creep in an Al-5.5 at.% Mg solid solution, Acta Metall. 22 (1974) 465-472.

[49] F.A. Mohamed, T.G. Langdon, The transition from dislocation climb to viscous glide in creep of solid solution alloys, Acta Metall. 22 (1974) 779-788.

[50] H. Oikawa, K. Sugawara, S. Karashima, High-temperature creep mechanism in an Al-2 at% Mg alloy determined by stress-relaxation tests, Scripta Metall. 10 (1976) 885-888.

[51] P. Yavari, F.A. Mohamed, T.G. Langdon, Creep and substructure formation in an Al-5% Mg solid solution alloy, Acta Metall. 29 (1981) 1495-1507.

[52] P. Yavari, T.G. Langdon, An examination of the breakdown in creep by viscous glide in solid solution alloys at high stress levels, Acta Metall. 30 (1982) 2181-2196.

[53] O.D. Sherby, P.M. Burke, Mechanical behavior of crystalline solids at elevated temperature, Prog. Mater. Sci. 13 (1968) 323-390.

[54] S.J. Rothman, N.L. Peterson, L.J. Nowicki, L.C. Robinson, Tracer diffusion of magnesium in aluminum single crystals, Phys. Status. Solidi. B 63 (1974) K29-K33.

[55] S. Komura, P.B. Berbon, M. Furukawa, Z. Horita, M. Nemoto, T.G. Langdon, High strain rate superplasticity in an Al-Mg alloy containing scandium, Scripta Mater. 38 (1998) 1851-1856.

[56] P.B. Berbon, S. Komura, A. Utsunomiya, Z. Horita, M. Furukawa, M. Nemoto, T.G. Langdon, An evaluation of superplasticity in aluminum-scandium alloys processed by equal-channel angular pressing, Mater. Trans. JIM 40 (1999) 772-778.

[57] Z. Horita, M. Furukawa, M. Nemoto, A.J. Barnes, T.G. Langdon, Superplastic forming at high strain rates after severe plastic deformation, Acta Mater. 48 (2000) 3633-3640.

[58] S. Komura, Z. Horita, M. Furukawa, M. Nemoto, T.G. Langdon, Influence of scandium on superplastic ductilities in an Al–Mg–Sc alloy, J. Mater. Res. 15 (2000) 2571-2576.

[59] H. Akamatsu, T. Fujinami, Z. Horita, T.G. Langdon, Influence of rolling on the superplastic behavior of an Al-Mg-Sc alloy after ECAP, Scripta Mater. 44 (2001) 759-764.

[60] M. Furukawa, A. Utsunomiya, K. Matsubara, Z. Horita, T.G. Langdon, Influence of magnesium on grain refinement and ductility in a dilute Al-Sc alloy, Acta Mater. 49 (2001) 3829-3838.

[61] S. Komura, M. Furukawa, Z. Horita, M. Nemoto, T.G. Langdon, Optimizing the procedure of equal-channel angular pressing for maximum superplasticity, Mater. Sci. Eng. A 297 (2001) 111-118.

[62] S. Komura, Z. Horita, M. Furukawa, M. Nemoto, T.G. Langdon, An evaluation of the flow behavior during high strain rate superplasticity in an Al-Mg-Sc alloy, Metall. Mater. Trans. A 32A (2001) 707-716.

[63] S. Lee, A. Utsunomiya, H. Akamatsu, K. Neishi, M. Furukawa, Z. Horita, T.G. Langdon, Influence of scandium and zirconium on grain stability and superplastic ductilities in ultrafine-grained Al-Mg alloys, Acta Mater. 50 (2002) 553-564.

[64] S. Ota, H. Akamatsu, K. Neishi, M. Furukawa, Z. Horita, T.G. Langdon, Low-temperature superplasticity in aluminum alloys processed by equal-channel angular pressing, Mater. Trans. 43 (2002) 2364-2369.

[65] G. Sakai, Z. Horita, T.G. Langdon, An evaluation of superplastic anisotropy after processing by equal-channel angular pressing, Mater. Trans. 45 (2004) 3079-3081.

[66] V.N. Perevezentsev, V.N. Chuvil'deev, A.N. Sysoev, V.I. Kopylov, T.G. Langdon, Achieving high-strain-rate superplasticity in Al-Mg-Sc-Zr alloys after severe plastic deformation, Phys. Met. Metall. 94 Suppl.1 (2002) S45-S53.

[67] V.N. Perevezentsev, V.N. Chuvil'deev, V.I. Kopylov, A.N. Sysoev, T.G. Langdon, Developing high strain rate superplasticity in Al-Mg-Sc-Zr alloys using equal-channel angular pressing, Ann. Chim.-Sci. Mat. 27 (2002) 99-109.

[68] Z. Horita, T.G. Langdon, Achieving exceptional superplasticity in a bulk aluminum alloy processed by high-pressure torsion, Scripta Mater. 58 (2008) 1029-1032.

[69] Y. Harai, K. Edalati, Z. Horita, T.G. Langdon, Using ring samples to evaluate the processing characteristics in high-pressure torsion, Acta Mater. 57 (2009) 1147-1153.

[70] M. Kawasaki, T.G. Langdon, Principles of superplasticity in ultrafine-grained materials, J. Mater. Sci. 42 (2007) 1782-1796.

[71] M. Kawasaki, T.G. Langdon, Review: achieving superplastic properties in ultrafine-grained materials at high temperatures, J. Mater. Sci. 51 (2016) 19-32.

[72] M. Schoenitz, E.L. Dreizin, Structure and properties of Al–Mg mechanical alloys, J. Mater. Res.18 (2003) 1827-1836.

[73] B. Ahn, A.P. Zhilyaev, H.-J. Lee, M. Kawasaki, T.G. Langdon, Rapid synthesis of an extra hard metal matrix nanocomposite at ambient temperature, Mater. Sci. Eng. A 635 (2015) 109-117.

[74] K. Lu, L. Lu, S. Suresh, Strengthening materials by engineering coherent internal boundaries at the nanoscale, Science 324 (2009) 349-352.

[75] T. Mukai, K. Higashi, S. Tanimura, Influence of the magnesium concentration on the relationship between fracture mechanism and strain rate in high purity Al-Mg alloys, Mater. Sci. Eng. A 176 (1994) 181-189.

[76] G.B. Burger, A.K. Gupta, P.W. Jeffrey, D.J. Lloyd, Microstructural control of aluminum sheet used in automotive applications, Mater. Charact. 35 (1995) 23-39.

[77] S. Shim, J.-I. Jang, G.M. Pharr, Extraction of flow properties of single-crystal silicon carbide by nanoindentation and finite-element simulation, Acta Mater. 56 (2008) 3824-3832.

[78] K.V. Rajulapati, R.O. Scattergood, K.L. Murty, Z. Horita, T.G. Langdon, C.C. Koch, Mechanical properties of bulk nanocrystalline aluminum-tungsten alloys, Metall. Mater. Trans. A 39A (2008) 2528–2534.

Figure captions

Figure 1 Variation of Vickers microhardness values along diameters of disks after HPT processing for different numbers of turns in an Al-3% Mg alloy: the lower dashed line denotes the hardness values before HPT processing of Hv ≈ 50 in the as-annealed condition.

Figure 2 Representative microstructures for the Al-3% Mg disks processed by HPT for, from the left, 1/4, 1, 5 and 10 turns. All microstructures were taken on the plane parallel to the disk surface either near the center at $r \approx 0$ mm (upper row) or close to the edge at $r \approx 3.5$ mm (lower row).

Figure 3 Average grain size with increasing equivalent strain at the edges of disks processed by HPT.

Figure 4 The XRD patterns over a limited 2 theta angular range for, from the top, compression under 6.0 GPa for 1 min without torsional straining and after HPT for 1/4, 1/2, 1, 5 and 10 turns.

Figure 5 Variation of the normalized peak intensity, K_i, for the major slip planes in the Al-3% Mg alloy with increasing numbers of HPT revolutions where $N = 0$ denotes the sample in compression for 1 min without torsional straining.

Figure 6 Variation of the lattice parameter of Al with increasing HPT turns where $N = 0$ denotes the sample in compression for 1 min without torsion.

Figure 7 Variations of dislocation density and area-weighted mean crystallite size as functions of the numbers of HPT turns and equivalent strain for the Al-3% Mg alloy where $N = 0$ denotes the sample in compression for 1 min without torsion.

Figure 8 Engineering stress-strain curves for the Al-3% Mg alloy in an annealed condition and after HPT processing through 5 and 10 turns after testing at a strain rate of 1.0×10^{-3} s^{-1} and at a temperature of 673 K.

Figure 9 Plots of elongation to failure (upper) and flow stress (lower) versus strain rate for the Al-3% Mg alloy in an annealed condition and after HPT processing through 5 and 10 turns after testing over a range of strain rates at a temperature of 673 K.

Figure 10 Plot of Vickers microhardness as a function of $d^{-1/2}$ for the Al-3% Mg alloy in an initial state without HPT, after HPT for 1/4, 1, 5 and 10 turns at the center and edge positions and after HPT followed by static annealing at 673 K for 1h: for comparison purposes, additional datum points are included for a similar Al-3% Mg alloy processed by ECAP [20] or HPT [19].

Table 1. Average grain size and standard deviation for Al-3% Mg alloy after HPT for 1/4, 1, 5 and 10 turns.

Location		Number of turns			
		1/4	1	5	10
Center	Grain size (nm)	1000	400	300	190
	Standard deviation	260	90	90	30
Edge	Grain size (nm)	600	240	220	180
	Standard deviation	180	90	60	30

Table 2. Grain sizes for Al-Mg alloys processed by HPT.

Material	HPT			Grain size (nm)	Reference
	Number of turns or strain	Pressure (GPa)	Temperature		
Al-1% Mg	10	6	RT	230	Andreau *et al.* [21]
Al-1.5% Mg	Logarithmic strain of 7	4	RT	150	Valiev *et al.* [25]
Al-1.5% Mg	Logarithmic strain of 7	5	RT	200-500	Ma *et al.* [26]
Al-3% Mg	Logarithmic strain of 7	5	RT	90	Furukawa *et al.* [19]
Al-3% Mg	10	6	RT	180-190	This investigation
Al-5% Mg	10	6	RT	~70-240	Bazarnik *et al.* [22]
Al-5% Mg	5	5	RT	150	Mazilkin *et al.* [23]
Al-10% Mg	5	5	RT	90	Mazilkin *et al.* [23]
Al-3% Mg-0.2% Sc	5	6	RT	150	Sakai *et al.* [27], Horita and Langdon [28]
Al-5.7% Mg-0.3% Sc	20	6	RT	100-200	Sauvage *et al.* [29]
Al-5.7% Mg-0.32% Sc-0.4% Mn	20	6	RT	100	Valiev *et al.* [30]
Al-5.9% Mg-0.3% Sc-0.3% Zr	5	6	RT	40-50	Dobatkin *et al.* [31]

Table 3. Mg concentration, hardness values by solution strengthening and contribution of solution strengthening to the total hardness for Al-3% Mg alloy after compression without torsion and after HPT for 1/4, 1/2, 1, 5 and 10 turns.

Condition	Compression	1/4 turn	1/2 turn	1 turn	5 turns	10 turns
Mg concentration (%)	1.94 ± 0.3	2.15 ± 0.3	2.59 ± 0.3	2.70 ± 0.3	3.70 ± 0.3	3.70 ± 0.3
Solution strengthening (Hv)	7.8 ± 0.6	9.8 ± 0.8	11.2 ± 0.9	11.7 ± 1.0	14.7 ± 1.2	14.7 ± 1.2
Contribution of solution strengthening to the total hardness (%)	-	8.1	7.2	6.8	8.2	8.2

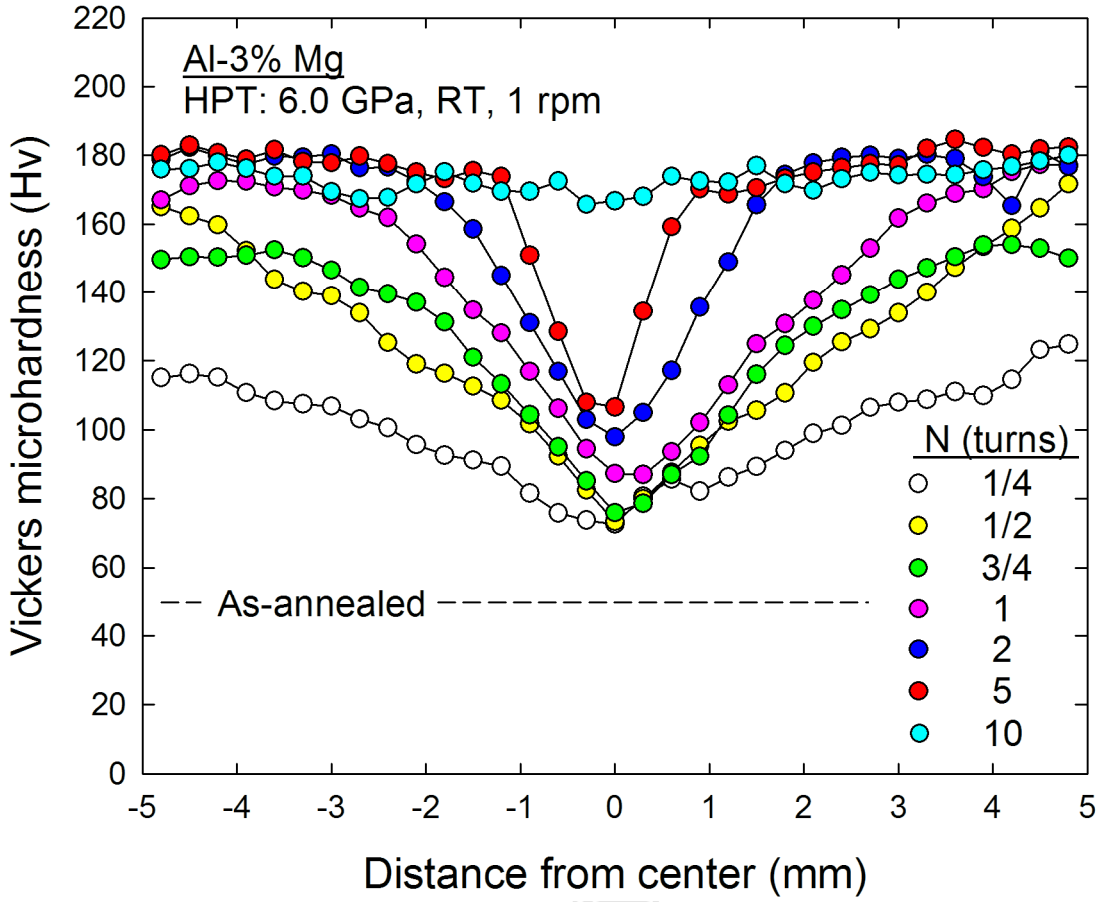

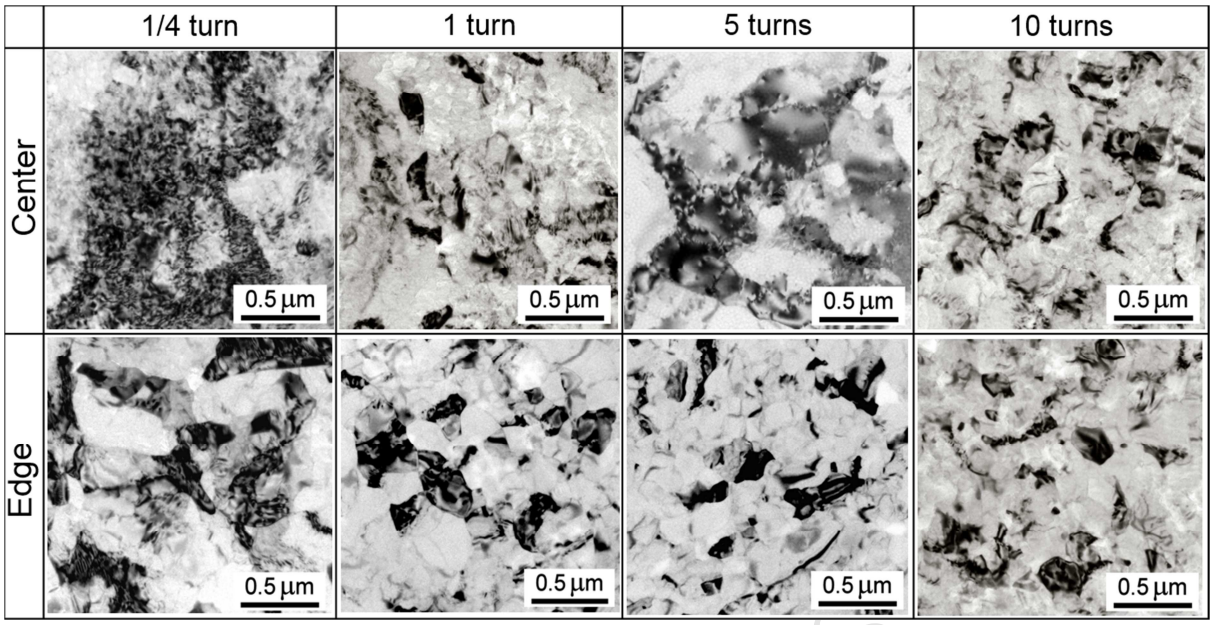

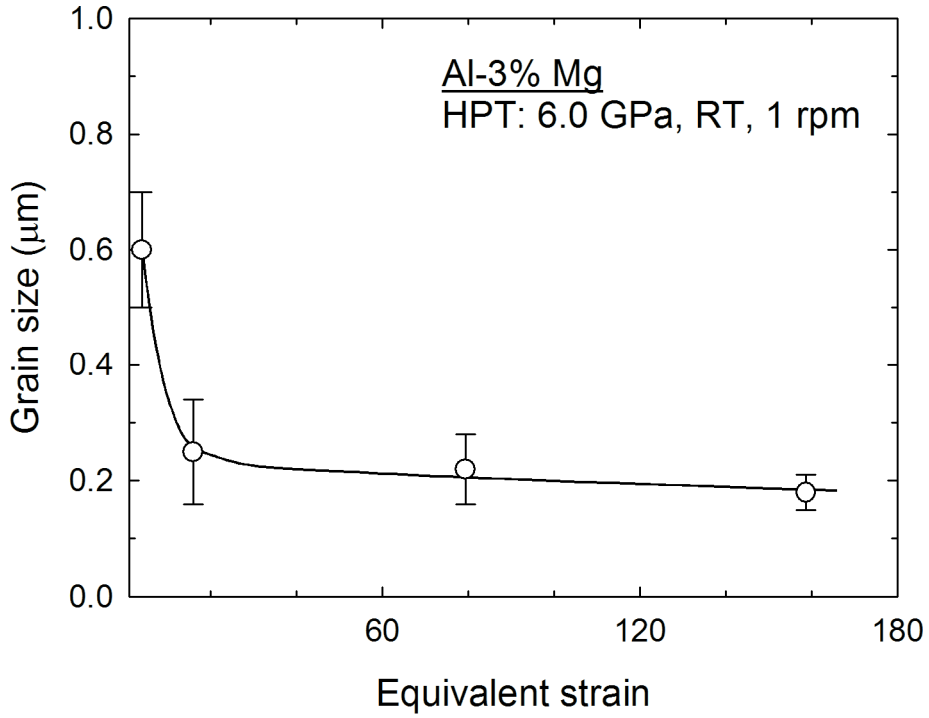

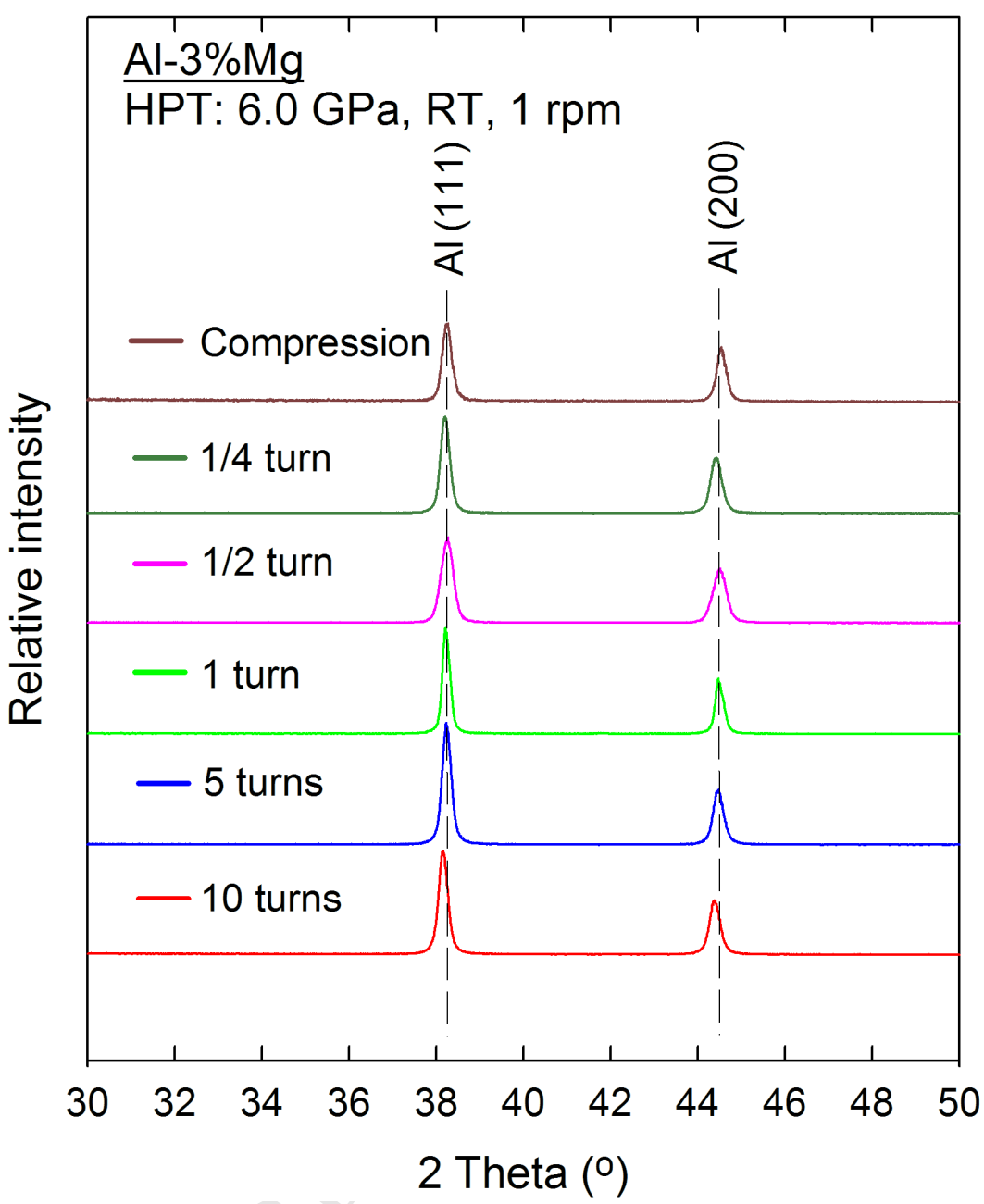
Al-3%Mg
HPT: 6.0 GPa, RT, 1 rpm
Al (111)
Al (200)
Compression
1/4 turn
1/2 turn
1 turn
5 turns
10 turns
Relative intensity
30
32
34
36
38
40
42
44
46
48
50
2 Theta (º)

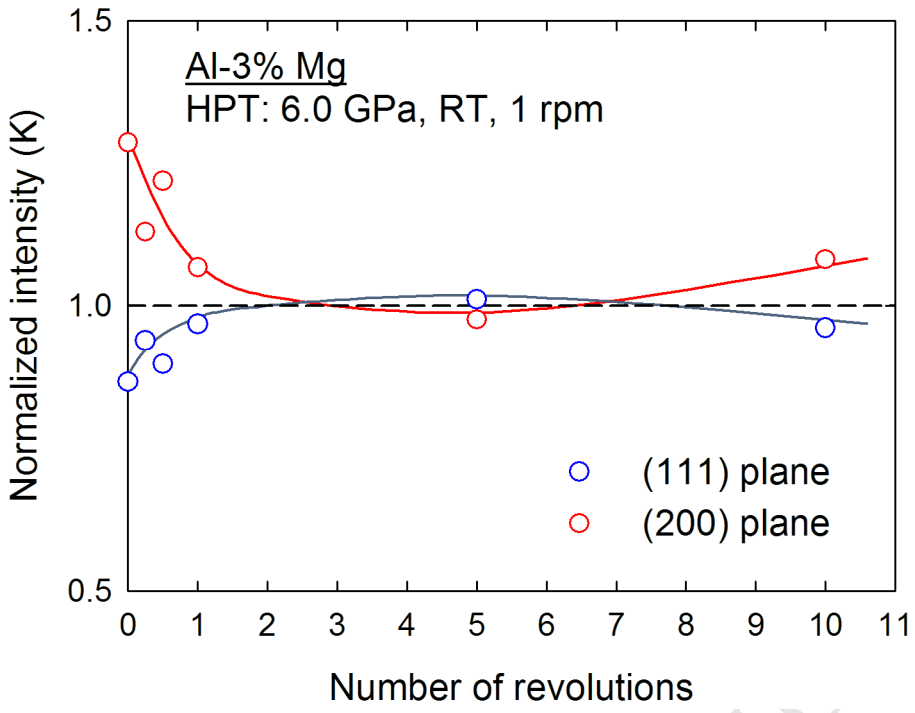

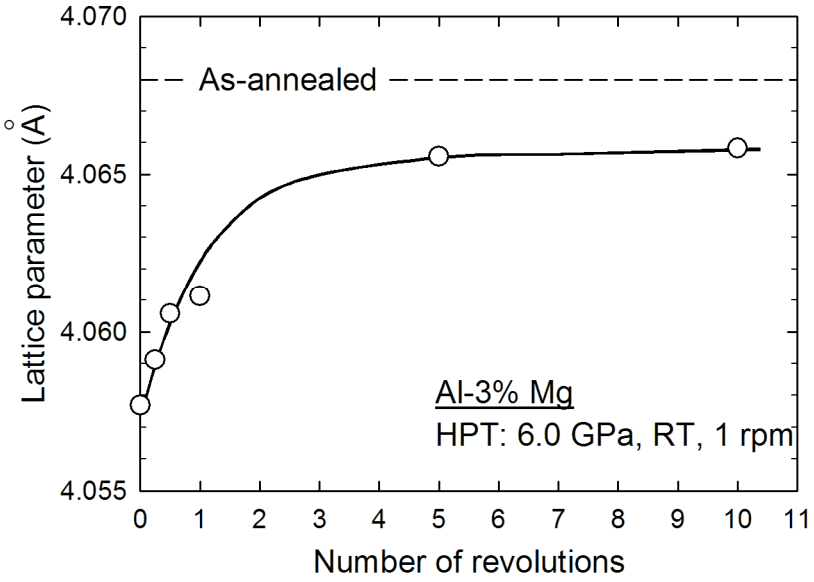

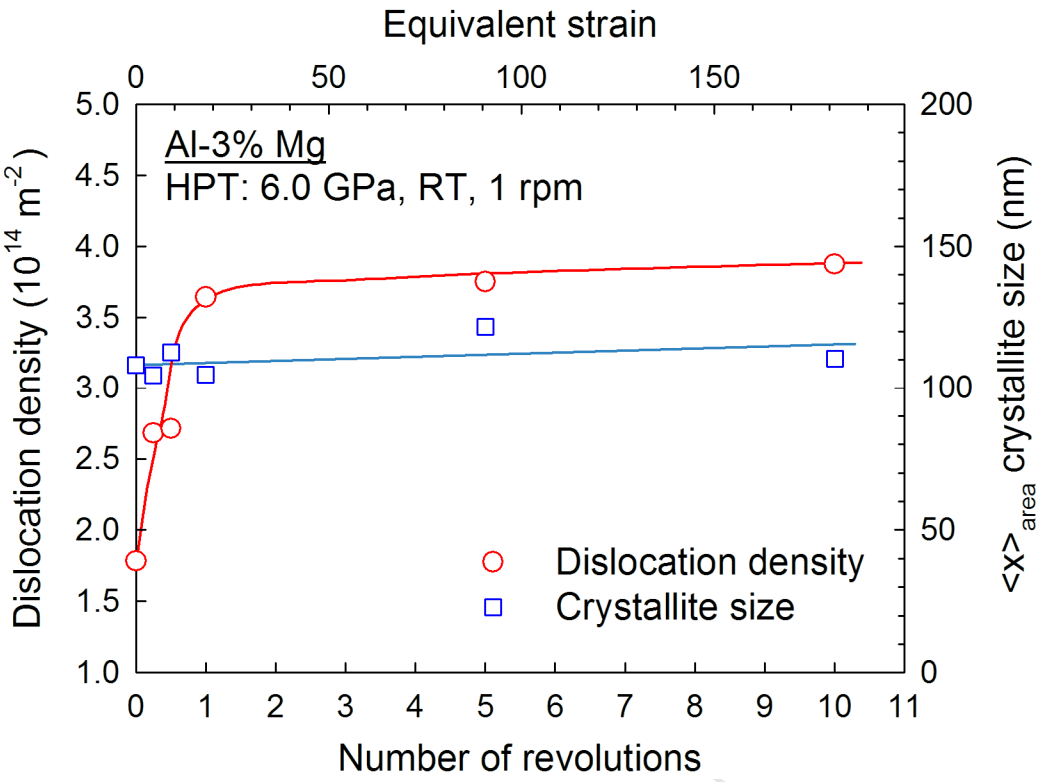

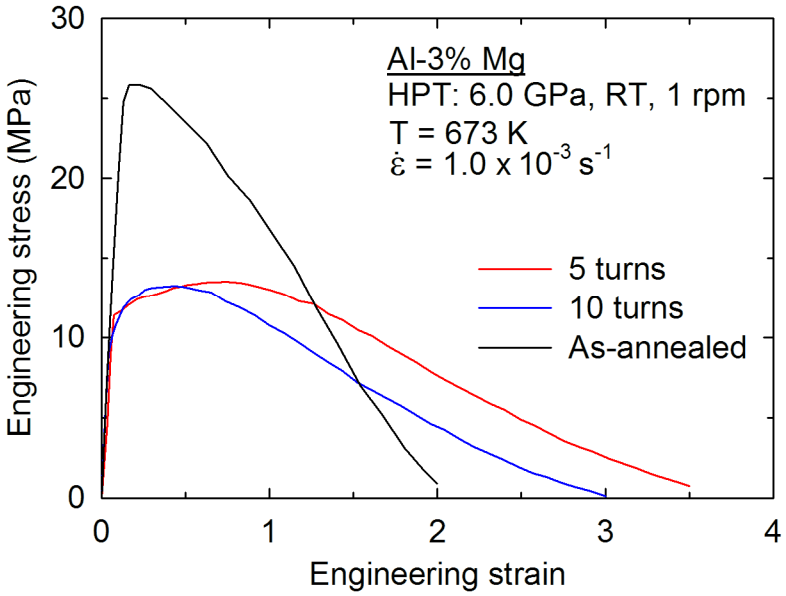

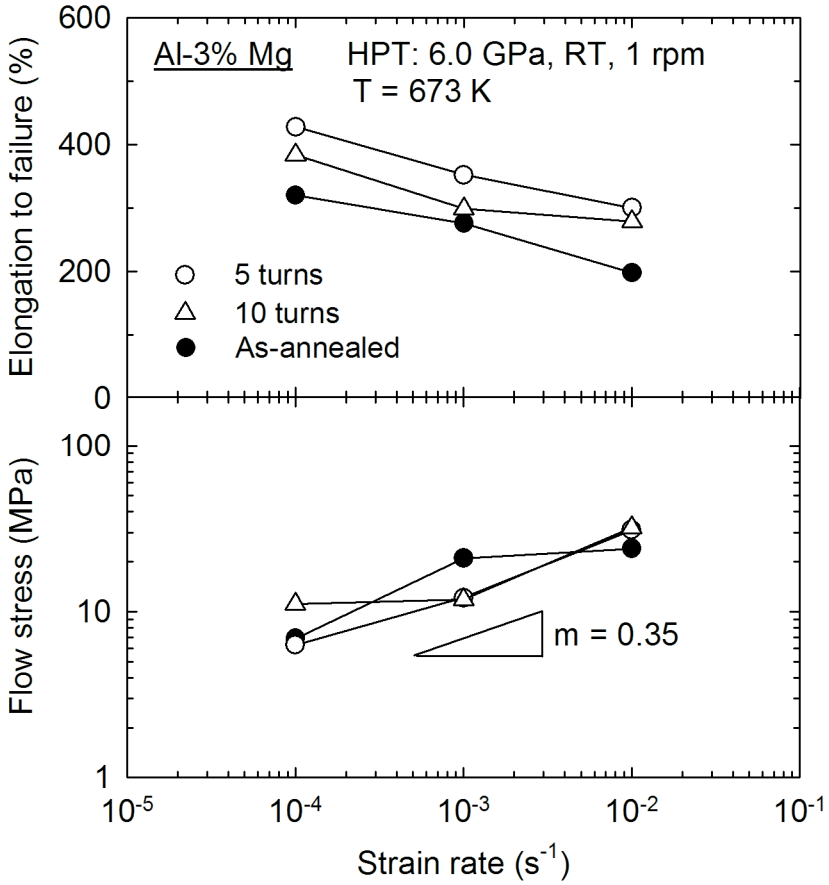

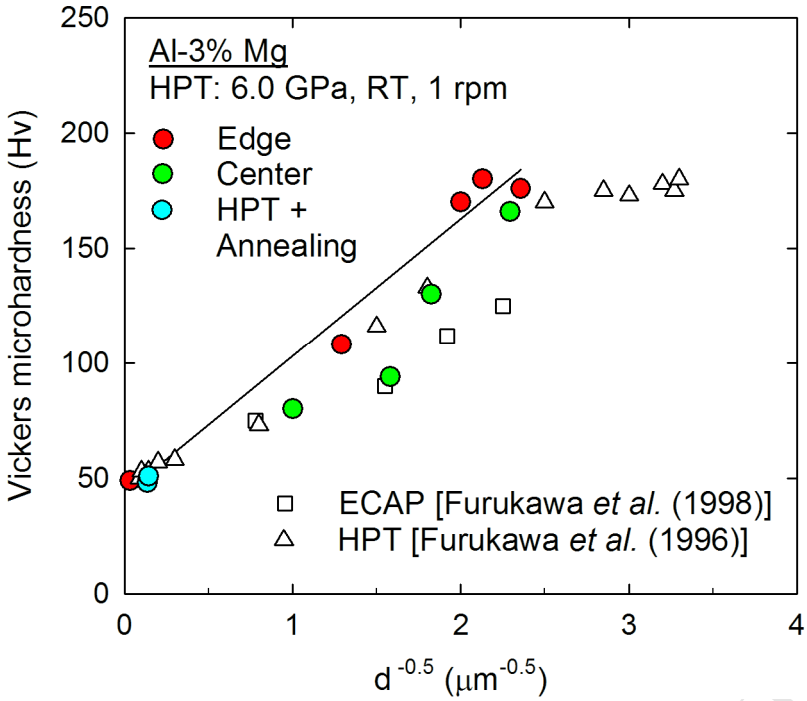

Highlights

- Significant grain refinement was achieved in Al-3% Mg by HPT through 10 turns.
- The evolution towards hardness homogeneity was observed after HPT for 10 turns.
- Microstructural evolution was examined with increasing HPT turns by XRD analysis.
- High-temperature flow of the Al-Mg alloy is controlled by viscous glide.
- Improved hardness through HPT is described mainly by the Hall-Petch relationship.